

On the curse of dimensionality for Normalizing Flows

Andrea Cocco^{1*}, Marco Letizia^{1,2*}, Humberto Reyes-González^{1,3*} and Riccardo Torre^{1*}


^{1*}INFN, Sezione di Genova, Via Dodecaneso 33, Genova, 16146, Italy.

^{2*}MaLGa - DIBRIS, University of Genova, Via Dodecaneso 35, Genova, 16146, Italy.

^{3*}Department of Physics, University of Genova, Via Dodecaneso 33, Genova, 16146, Italy.

*Corresponding author(s). E-mail(s): andrea.cocco@ge.infn.it;
marco.letizia@edu.unige.it; humbertoalonso.reyesgonzalez@edu.unige.it;
riccardo.torre@ge.infn.it;

Abstract

Normalizing Flows have emerged as a powerful brand of generative models, as they not only allow for efficient sampling of complicated target distributions, but also deliver density estimation by construction. We propose here an in-depth comparison of coupling and autoregressive flows, both of the affine and rational quadratic spline type, considering four different architectures: Real-valued Non-Volume Preserving (RealNVP), Masked Autoregressive Flow (MAF), Coupling Rational Quadratic Spline (C-RQS), and Autoregressive Rational Quadratic Spline (A-RQS). We focus on different target distributions of increasing complexity with dimensionality ranging from 4 to 1000. The performances are discussed in terms of different figures of merit: the one-dimensional Wasserstein distance, the one-dimensional Kolmogorov-Smirnov test, the Frobenius norm of the difference between correlation matrices, and the training time. Our results indicate that the A-RQS algorithm stands out both in terms of accuracy and training speed. Nonetheless, all the algorithms are generally able, without much fine-tuning, to learn complex distributions with limited training data and in a reasonable time, of the order of hours on a Tesla V100 GPU. The only exception is the C-RQS, which takes significantly longer to train, and does not always provide good accuracy. All algorithms have been implemented using TENSORFLOW2 and TENSORFLOW PROBABILITY and made available on GITHUB .

Keywords: Machine Learning, Generative Models, Density Estimation, Normalizing Flows

Contents

1	Introduction	2
2	Normalizing Flows	3
2.1	Coupling flows	4
2.2	Autoregressive flows	5
3	Architectures	5
3.1	The RealNVP	6
3.2	The MAF	6
3.3	The RQS bijector	6
3.4	The C-RQS	7
3.5	The A-RQS	7
4	Non-parametric quality metrics	8
5	Testing the Normalizing Flows	9
5.1	Correlated Mixture of Gaussians .	9
5.2	Extremely multi-modal CMoG . .	10
5.3	Truncated Gaussians	11
6	Conclusions and Outlook	13
A	Implementation of NF architectures	14
A.1	The RealNVP	14
A.2	The MAF	14
A.3	The C-RQS	15
A.4	The A-RQS	16
B	Hyperparameters	16
C	Correlated mixture of Gaussians	17
D	Extremely multimodal correlated mixture of Gaussians	18
E	Truncated Gaussians	19
F	Corner plots	20

1 Introduction

Since a few years now, the High Energy Physics (HEP) community has started to substantially explore Machine Learning techniques for a diverse variety of tasks and, as such, a large number of ideas, applications, and tools are being published [1, 2]. This is not only the case within experimental collaborations, but also among the phenomenology and formal theory communities

[3–6]. Even more, as we head towards the High-Luminosity era of the Large Hadron Collider (HL-LHC), in which unprecedented amount of highly complex data need to be simulated, collected, and finally analyzed, the importance of building reliable and more efficient methods, techniques, and workflows for HEP is becoming compulsory. As the community has already realized, ML plays a crucial role in this development. In particular, ML provides a potential solution to meet the expected computing resources for simulating and reconstructing the products of the collisions and will also be essential for developing novel strategies for triggering and reconstructing data, as well as for the statistical analysis, interpretation, and preservation of such data. This represents a brand new field of research, that effectively complements the HL-LHC physics programme. Furthermore, supported by the largely enhanced precision expected at the HL-LHC, dedicated ML methods will provide great opportunities to pursue data-driven searches, i.e. for anomaly detection, data quality monitoring and efficient background estimation. However, to ensure a systematic implementation of ML methods in the HEP workflows, one needs to carefully study their properties and capabilities against complex, high-dimensional data and to assess their ability to match the required precision, typically much higher than that of industrial and “real-life” applications. This program, which can go under the name of “Precision ML”, cannot be separated from the development of reliable quality metrics and proper assessment of uncertainties.

Here we focus on Normalizing Flows (NFs) [7–10], a class of neural density estimators that, on one side offers a competitive approach to generative models, such as Generative Adversarial Networks (GAN) [11] and Variational AutoEncoders (VAE) [12, 13], for the generation of synthetic data, and, on the other side, opens up a wide range of applications due to its ability to directly perform density estimation. While applications of the generative direction of NFs is rather obvious in a field like HEP, which poses its foundations on Monte Carlo simulations, it is interesting to mention some of the possible density estimation applications. The ability to directly learn the Likelihood, or the posterior in a Bayesian framework, has applications ranging from analysis inference, reinterpretation, and preservation, to

simulation-based likelihood-free inference [14–19], to unfolding of HEP analyses [20], to the generation of effective priors for Bayesian inference [21–26] and systematic uncertainty estimation and parametrization, or effective proposals for sequential Monte Carlo [27–32], numerical integration based on importance sampling algorithms [33–36], and probabilistic programming applied to fast inference [37, 38].

The basic principle behind NFs is to perform a series of invertible bijective transformations on a simple base distribution to approximate the complex distribution of interest. The optimal parameters of the transformations, often called bijectors, are derived from training Neural Networks (NNs) that directly take the negative log-likelihood of the true data computed with the NF distribution as the loss function. As it turns out, PDFs are everywhere in HEP: from the likelihood function of an experimental or phenomenological result, to the distribution that describes a particle-collision process. Furthermore, it has been shown that directly using the likelihood as loss function, leads to a more stable learning process, making NFs very efficient sample generators. Thus, NFs have found numerous applications in HEP: they have been used for numerical integration and event generation [39–43], anomaly detection [44–46], detector unfolding [47, 48], etc. This growing interest in NFs implies the urgency of testing state-of-the-art NF architectures against complex high-dimensional data to ensure their systematic usability and to assess their expected performances, which is the purpose of the present study. By testing NFs against generic complex distributions of increasing dimensionality, we aim to make a step forward in the general understanding of the performances and properties of NFs applied to high dimensional data.

Our strategy is the following. We implemented and tested four of the mostly used NF architectures of the coupling and autoregressive type: Real-valued Non-Volume Preserving (RealNVP) [49], Masked Autoregressive Flow (MAF) [50], Coupling Rational Quadratic Spline (C-RQS) [51], and Autoregressive Rational Quadratic Spline (A-RQS) [51]. We tested these NF architectures against three types of target distributions with dimensionalities ranging from 4 to 1000: Correlated Mixture of Gaussians (CMoG), Extremely Multimodal Correlated Mixture of Gaussians

(CMoGem), and Truncated Gaussians (TG). We also performed a small-scale hyperparameter scan, explicitly avoiding to fine-tune the models, and provide the best result for each NF architecture and target distribution. The performances were measured by means of several figures of merit: the median (over dimensions) 1D Wasserstein distance, the median (over dimensions) p -value of 1D Kolmogorov-Smirnov tests, the Frobenius norm of the difference of the correlation matrices, and the training time.

The paper is organized as follows. In Section 2 we describe the concept of NFs in more detail, focusing on the coupling and autoregressive types. In Section 3 we introduce the specific NF architectures under investigation. In Section 4 we present the metrics used in our analysis and in Section 5 we discuss our results. Finally, we provide our concluding remarks in Section 6, with emphasis on the several prospective research avenues that we plan to follow.

2 Normalizing Flows

Normalizing Flows are made of series of bijective, continuous, and invertible transformations that map a simple *base* PDF to a more complicated *target* PDF. The purpose of NFs is to estimate the unknown underlying distribution of some data of interest and to allow the generation of samples approximately following the same distribution. Since the parameters of both the base distribution and the transformations are known, one can *generate* samples from the target distribution by drawing samples from the base distribution and then applying the proper transformation. This is known as the *generative direction* of the flow. Furthermore, since the NF transformations are invertible, one can also obtain the probability density of the true samples, via inverse transformations from the target to the base PDF. This is known as the *normalizing direction* of the flow. It is called “normalizing” because the base distribution is often Gaussian, even though this is not a requirement, and this is also the origin of the name Normalizing Flows.

The basic idea behind NFs is the change of variable formula for a PDF. Let $X, Y \in \mathbb{R}^D$ be random variables with PDFs $p_X, p_Y : \mathbb{R}^D \rightarrow \mathbb{R}$. Let us define a bijective map $\mathbf{g} : X \rightarrow Y$, with

inverse $\mathbf{f} = \mathbf{g}^{-1}$.¹ The two densities are then related by the well known formula

$$\begin{aligned} p_Y(y) &= p_X(\mathbf{g}^{-1}(y)) |\det \mathbf{J}_g|^{-1} \\ &= p_X(\mathbf{f}(y)) |\det \mathbf{J}_f|, \end{aligned} \quad (1)$$

where $\mathbf{J}_f = \frac{\partial \mathbf{f}}{\partial y}$ is the Jacobian of $\mathbf{f}(y)$ and $\mathbf{J}_g = \frac{\partial \mathbf{g}}{\partial x}$ is the Jacobian of $\mathbf{g}(x)$.

Let us now consider a set of parameters $\{\phi\}$ characterizing the chosen base density p_X (typically the mean vector and covariance matrix of a multivariate Gaussian) and parametrize the map \mathbf{g} by another set of parameters $\{\theta\}$. One can then perform a maximum likelihood estimation of the parameters $\Phi = \{\phi, \theta\}$ given some measured data $\mathcal{D} = \{y^{(i)}\}_{i=1}^M$ distributed according to the unknown PDF p_y . The log-likelihood of the data is given by the following expression

$$\begin{aligned} \log p(\mathcal{D} | \Phi) &= \sum_{i=1}^M \log p_Y(y^{(i)} | \Phi) \\ &= \sum_{i=1}^M \log p_X(\mathbf{f}(y^{(i)}; \theta) | \theta, \phi) + \log |\det \mathbf{J}_f|, \end{aligned} \quad (2)$$

where we made the dependence of \mathbf{f} on θ explicit through the notation \mathbf{f}_θ . Then, the best estimate of the parameters Φ is given by

$$\hat{\Phi} = \arg \max_{\Phi} \log p(\mathcal{D} | \Phi). \quad (3)$$

Once the parameters $\hat{\Phi}$ have been estimated from the data, one can sample the estimated target distribution by sampling the base PDF and applying the generative map \mathbf{g} . The normalizing direction \mathbf{f} can instead be used to perform density evaluation by transforming the new data of interest into sample generated by the base PDF, which is easier to evaluate.

Beside being invertible, the map \mathbf{g} should satisfy the following properties:

- it should be sufficiently expressive to appropriately model the target distribution;

- it should be computationally efficient, that means that both \mathbf{f} (for training, that means computing the likelihood) and \mathbf{g} (for generating samples), as well as their Jacobian determinants must be easily calculable.

The composition of invertible bijective functions is also an invertible bijective function. Thus, \mathbf{g} can be generalized to a set of N transformations as $\mathbf{g} = g_N \circ g_{N-1} \circ \dots \circ g_1$ with inverse $\mathbf{f} = f_1 \circ \dots \circ f_{N-1} \circ f_N$ and $\det \mathbf{J}_f = \prod_{i=1}^N \det \mathbf{J}_{f_i}$, where each \mathbf{f}_i depends on a y_i intermediate random variable. This is a standard strategy to increase the flexibility of the overall transformation.

Typically, but not mandatorily, NF models are implemented using NNs to determine the parameters of the bijectors. The optimal values are obtained by minimizing a loss function corresponding to minus the log-likelihood defined as in Eq. 2. This makes the models extremely flexible, with a usually stable training, at the cost of a potentially large number of parameters. Nonetheless, the flow transformation must be carefully designed, for instance, even if a given map and its inverse, with their respective Jacobians, are computable, one direction might be more efficient than the other, leading to models that favor sampling over evaluation (and training) or vice-versa. Among the wide and growing variety of NF architectures available, see Ref. [52] for an overview, we focus in this work on *coupling* [10] and *autoregressive* flows [53], arguably the most widely used implementations of NFs, particularly in HEP.

2.1 Coupling flows

Coupling flows, originally introduced in Ref. [10], are made of stacks of so-called coupling layers, in which a distribution with dimensionality D is partitioned in two parts A and B with dimensionalities d and $D-d$, respectively. The parameters of the bijector transforming dimensions A are modeled by a NN that uses B as input; effectively constructing $p(y_d | x_{d-D})$ conditional probability distributions. At each coupling layer, different partition combinations are applied, such that the full distribution is properly transformed.

In other words, starting from a disjoint partition of a random variable $Y \in \mathbb{R}^D$ such that $(y^A, y^B) \in \mathbb{R}^d \times \mathbb{R}^{D-d}$ and a bijector $\mathbf{h}(\cdot; \theta) : \mathbb{R}^d \rightarrow \mathbb{R}^d$, a coupling layer maps $\mathbf{g} : X \rightarrow Y$ as

¹Throughout the paper we always interpret X as the base distribution and Y as the target distribution, i.e. the data. We also always model flows in the generative direction, from base to data.

follows

$$\begin{aligned} y^A &= \mathbf{h}(x^A; \Theta(x^B)), \\ y^B &= x^B, \end{aligned} \quad (4)$$

where the parameters θ are defined by a generic function $\Theta(x^B)$ only defined on the \mathbb{R}^{D-d} partition, generally modeled by a NN. The function $\Theta(x^B)$ is called a *conditioner*, while the bijectors \mathbf{h} and \mathbf{g} are called *coupling function* and *coupling flow*, respectively. The necessary and sufficient condition for the coupling flow \mathbf{g} to be invertible is that the coupling function \mathbf{h} is invertible. In this case the inverse transformation is given by

$$\begin{aligned} x^A &= \mathbf{h}^{-1}(y^A; \Theta(x^B)), \\ x^B &= y^B, \end{aligned} \quad (5)$$

The Jacobian of \mathbf{g} is then a two block triangular matrix. For the dimensions $\{1 : d\}$, is given by the Jacobian of \mathbf{h} , and for dimensions $\{d : D\}$ is the identity matrix. Thus, the Jacobian determinant is just

$$\det J_g = \prod_{i=1}^d \frac{\partial h_i}{\partial x_i^A}. \quad (6)$$

Note that the choice of the partition is arbitrary. The most common choice is to split the dimensions in half, but other partitions are possible [52].

2.2 Autoregressive flows

Autoregressive flows, first introduced in Ref. [53], can be viewed as a generalization of coupling flows. Now, the transformations of each dimension i are modeled by an autoregressive DNN according to the previously transformed dimensions of the distribution, resulting in the $p(y_i | y_{1:i-1})$ conditional probability distributions, where $y_{1:i-1}$ is a shorthand notation to indicate the list of variables y_1, \dots, y_{i-1} . After each autoregressive layer, the dimensions are permuted, to ensure the expressivity of the bijections over the full dimensionality of the target distribution.

Let us consider a bijector $\mathbf{h}(\cdot; \theta) : \mathbb{R} \rightarrow \mathbb{R}$, parametrized by θ . We can define an autoregressive flow function \mathbf{g} such that

$$\begin{aligned} y_1 &= x_1, \\ y_i &= \mathbf{h}(x_i; \Theta_i(y_{1:i-1})), \quad i = 2, \dots, D. \end{aligned} \quad (7)$$

The resulting Jacobian of \mathbf{g} is again a triangular matrix, whose determinant is easily computed as

$$\det J_g = \prod_{i=1}^D \frac{\partial h_i}{\partial x_i}. \quad (8)$$

where $\partial h_i / \partial x_i$ are the diagonal terms of the Jacobian.

Given the structure of the bijector similar to the coupling flow, also in this case the bijector is referred to as a *coupling function*. Note that Θ_j can also be alternatively determined with the precedent untransformed dimensions of X [53], such that

$$\begin{aligned} y_1 &= x_1, \\ y_i &= \mathbf{h}(x_i; \Theta_i(x_{1:i-1})), \quad i = 2, \dots, D. \end{aligned} \quad (9)$$

The choice of variables used to model the conditioner may depend on whether the NF is intended for sampling or density estimation. In the former case, Θ is usually chosen to be modeled from the base variable X , so that the transformations in the generative direction would only require one forward pass through the flow. The transformations in the normalizing direction would instead require D iterations through the autoregressive architecture. This case is referred to as *inverse autoregressive flow*² [53] and corresponds to the transformations in Eq. (9). Conversely, in the case of density estimation, it is convenient to parametrize the conditioner using the target variable Y , since transformations would be primarily in the normalizing direction. This case is referred to as *direct autoregressive flow* and corresponds to the transformations in Eq. (7). In any case, when training the NFs one always needs to perform the normalizing transformations to estimate the log-likelihood of the data, as in Eq. 2. In our study, we only consider the direct autoregressive flow described by Eq. (7).

3 Architectures

In the previous section we have described NFs, focusing on the two most common choices for

²Notice that Ref. [52], parametrizing the flow in the normalizing direction (the opposite of our choice), apparently uses the inverse of our formulas for direct and inverse flows. Our notation (and nomenclature) is consistent with Ref. [50].

parametrizing the bijector \mathbf{g} in terms of the coupling function \mathbf{h} . The only missing ingredient to make NFs concrete, remains the explicit choice of \mathbf{h} . For this study, we have chosen four of the most popular implementations of coupling and autoregressive flows: the Real-valued Non-Volume Preserving (RealNVP) [49], the Masked Autoregressive Flow (MAF) [50], and the Coupling and Autoregressive Rational-Quadratic Neural Spline Flows (C-RQS and A-RQS) [51].³ We discuss them in turn in the following subsections and give additional details about our specific implementation in Appendices A.1-A.4.

3.1 The RealNVP

The RealNVP [49] is a type of coupling flow whose coupling functions \mathbf{h} are affine functions with the following form:

$$\begin{aligned} y_i &= x_i, & i &= 1, \dots, d, \\ y_i &= x_i e^{s_{i-d}(x_{1:d})} + t_{i-d}(x_{1:d}), & i &= d+1, \dots, D, \end{aligned} \quad (10)$$

where the s and t functions, defined on $\mathbb{R}^d \rightarrow \mathbb{R}^{D-d}$, respectively correspond to the scale and translation transformations modeled by NNs. The product in Eq. (10) is intended elementwise for each i so that, x_{d+1} is multiplied by s_1 , x_{d+2} by s_2 , and so on, up to x_D , which is multiplied by s_{D-d} . The Jacobian of this transformation is a triangular matrix with diagonal

$\text{diag}(\mathbb{I}_d, \text{diag}(\exp(s_i(x_{1:d}))))$ with $i = d+1, \dots, D$, so that its determinant is independent of t and simply given by

$$\det J = \prod_{i=1}^{D-d} e^{s_i(x_{1:d})} = \exp\left(\sum_{i=1}^{D-d} s_i(x_{1:d})\right). \quad (11)$$

$$\begin{aligned} x_i &= y_i, & i &= 1, \dots, d, \\ x_i &= (y_i - t_{i-d}(y_{1:d})) e^{-s_{i-d}(y_{1:d})}, & i &= d+1, \dots, D. \end{aligned} \quad (12)$$

A crucial property of the affine transformation (10) is that its inverse (12) is again an affine transformation depending only on s and t , and not on

their inverse. This implies that the s and t functions can be arbitrarily complex (indeed they are parametrized by a DNN), still leaving the RealNVP equally efficient in the forward (generative) and backward (normalizing) directions.

3.2 The MAF

The MAF algorithm was developed starting from the Masked Autoencoder for Distribution Estimation (MADE) [54] approach for implementing an autoregressive Neural Network through layers masking (see Appendix A.2).

In the original MAF implementation [50], the bijectors are again affine functions described as

$$\begin{aligned} y_1 &= x_1, \\ y_i &= x_i e^{s_{i-1}(y_{1:i-1})} + t_{i-1}(y_{1:i-1}), \quad i = 2, \dots, D. \end{aligned} \quad (13)$$

The functions s and t are now defined on $\mathbb{R}^{D-1} \rightarrow \mathbb{R}^{D-1}$. The determinant of the Jacobian is simply

$$\det J = \prod_{i=1}^{D-1} e^{s_i(y_{1:i})} = \exp\left(\sum_{i=1}^{D-1} s_i(y_{1:i})\right) \quad (14)$$

and the inverse transformation is

$$\begin{aligned} x_1 &= y_1, \\ x_i &= (y_i - t_{i-1}(y_{1:i-1})) e^{-s_{i-1}(y_{1:i-1})}, \quad i = 2, \dots, D. \end{aligned} \quad (15)$$

As in the case of the RealNVP, the affine transformation guarantees that the inverse transformation only depends on s and t and not on their inverse, allowing for the choice of arbitrarily complex functions without affecting computational efficiency.

3.3 The RQS bijector

The bijectors in a coupling or masked autoregressive flow are not restricted to affine functions. It is possible to implement more expressive transformations as long as they remain invertible and computationally efficient. This is the case of the so-called Rational-Quadratic Neural Spline Flows [51].

The spline bijectors are made of K bins, where in each bin one defines a monotonically-increasing rational-quadratic function. The binning is defined on an interval $\mathbb{B} = [-B, B]$, outside of which the function is set to the identity transformation. The bins are defined by a set of

³Reference [51] refers to coupling and autoregressive RQS flows as RQ-NSF (C) and RQ-NSF (AR), where RQ-NSF stands for Rational-Quadratic Neural Spline Flows, and A and C for autoregressive and coupling, respectively.

$K + 1$ coordinates $\{(x_i^{(k)}, y_i^{(k)})\}_{k=0}^K$, called *knots*, monotonically increasing between $\{(x_i^{(0)}, y_i^{(0)}) = (-B, -B)$ to $\{(x_i^{(K)}, y_i^{(K)}) = (B, B)$. We use the bracket index notation to denote knots coordinates, which are defined for each dimension of the vectors x_i and y_i . It is possible to construct a rational-quadratic spline bijector with the desired properties with the following procedure [55].

Let us define the quantities

$$\begin{aligned} h_i^{(k)} &= x_i^{(k+1)} - x_i^{(k)}, \\ \Delta_i^{(k)} &= (y_i^{(k+1)} - y_i^{(k)})/h_i^{(k)}. \end{aligned} \quad (16)$$

Obviously, $\Delta_i^{(k)}$ represents the variation of y_i with respect to the variation of x_i within the k -th bin. Moreover, since we assumed monotonically increasing coordinates, $\Delta_i^{(k)}$ is always positive or zero. We are interested in defining a bijector $\mathbf{g}(x_i)$, mapping the \mathbb{B} interval to itself, such that $\mathbf{g}(x_i^{(k)}) = y_i^{(k)}$, and with derivatives $d_i^{(k)} = dy_i^{(k)}/dx_i^{(k)}$ satisfying the conditions

$$\begin{aligned} d_i^{(k)} &= d_i^{(k+1)} = 0 \quad \text{for } \Delta_i^{(k)} = 0, \\ d_i^{(k)}, d_i^{(k+1)} &> 0 \quad \text{for } \Delta_i^{(k)} > 0, \end{aligned} \quad (17)$$

necessary, and also sufficient, in the case of a rational quadratic function, to ensure monotonicity [55]. Moreover, for the boundary knots, we set $d_i^{(0)} = d_i^{(K)} = 1$ to match the linear behavior outside the \mathbb{B} interval.

For $x_i \in [x_i^{(k)}, x_i^{(k+1)}]$ we define

$$\theta_i = (x_i - x_i^{(k)})/h_i^{(k)}, \quad (18)$$

such that $\theta_i \in [0, 1]$. Then, for x_i in each of the intervals $[x_i^{(k)}, x_i^{(k+1)}]$ with $k = 0, \dots, K - 1$, we define

$$y_i = P_i^{(k)}(\theta_i)/Q_i^{(k)}(\theta_i), \quad (19)$$

with the functions P and Q defined by

$$\begin{aligned} P_i^{(k)}(\theta_i) &= \Delta_i^{(k)} y_i^{(k+1)} \theta_i^2 + \Delta_i^{(k)} y_i^{(k)} (1 - \theta_i)^2 \\ &\quad + (y_i^{(k)} d_i^{(k+1)} + y_i^{(k+1)} d_i^{(k)}) \theta_i (1 - \theta_i), \\ Q_i^{(k)}(\theta_i) &= \Delta_i^{(k)} + (d_i^{(k+1)} + d_i^{(k)} - 2\Delta_i^{(k)}) \theta_i (1 - \theta_i). \end{aligned} \quad (20)$$

The ratio in Eq. (19) can then be written in the simplified form

$$y_i = y_i^{(k)} + \frac{(y_i^{(k+1)} - y_i^{(k)})(\Delta_i^{(k)} \theta_i^2 + d_i^{(k)} \theta_i (1 - \theta_i))}{\Delta_i^{(k)} + (d_i^{(k+1)} + d_i^{(k)} - 2\Delta_i^{(k)}) \theta_i (1 - \theta_i)}. \quad (21)$$

The Jacobian $\mathbf{J}_{\mathbf{g}} = \partial y_i / \partial x_j$ is then diagonal, with entries given by

$$\frac{(\Delta_i^{(k)})^2 (d_i^{(k+1)} \theta_i^2 + 2\Delta_i^{(k)} \theta_i (1 - \theta_i) + d_i^{(k)} (1 - \theta_i)^2)}{(\Delta_i^{(k)} + (d_i^{(k+1)} + d_i^{(k)} - 2\Delta_i^{(k)}) \theta_i (1 - \theta_i))^2}, \quad (22)$$

for $i = 1, \dots, D$. The inverse of the transformation (19) can also be easily computed by solving the quadratic Eq. (19) with respect to x_i .

In practice, B and K are fixed variables (hyperparameters), while $\{(x_i^{(k)}, y_i^{(k)})\}_{k=0}^K$ and $\{d_i^{(k)}\}_{k=1}^{K-1}$ are $2(K + 1)$ plus $K - 1$ parameters, modeled by a NN, which determine the shape of the spline function. The different implementations of the RQS bijector, in the context of coupling and autoregressive flows, are determined by the way in which such parameters are computed. We briefly describe them in turn in the following two subsections.

3.4 The C-RQS

In the coupling flow case (C-RQS), one performs the usual partitioning of the D dimensions in the two sets composed of the first d and last $D - d$ dimensions. The first d dimensions are then kept unchanged $y_i = x_i$ for $i = 1, \dots, d$, while the parameters describing the RQS transformations of the other $D - d$ dimensions are determined from the inputs of the first d dimensions, denoted by $x_{1:d}$. Schematically, we could write

$$\begin{aligned} x_i^{(k)} &= x_i^{(k)}(x_{1:d}), \\ y_i^{(k)} &= y_i^{(k)}(x_{1:d}), \\ d_i^{(k)} &= d_i^{(k)}(x_{1:d}), \end{aligned} \quad (23)$$

for $i = d + 1, \dots, D$.

A schematic description of our implementation of the C-RQS is given in Appendix A.3.

3.5 The A-RQS

The RQS version of the MAF, that we call A-RQS, is instead obtained leaving unchanged the first

dimension $y_1 = x_1$ and determining the parameters of the transformation of the i -th dimension from the output of all preceding dimensions, denoted by $y_{1:i-1}$. Schematically, this is given by

$$\begin{aligned} x_i^{(k)} &= x_i^{(k)}(y_{1:i-1}), \\ y_i^{(k)} &= y_i^{(k)}(y_{1:i-1}), \\ d_i^{(k)} &= d_i^{(k)}(y_{1:i-1}), \end{aligned} \quad (24)$$

for $i = 2, \dots, D$.

4 Non-parametric quality metrics

We evaluate the performances of the different algorithms in terms of a few figures of merit: median of p -values of 1D Kolmogorov-Smirnov (KS) tests, median of 1D Wasserstein distances (W-distance), and Frobenius norm (F-norm) of the difference of the correlation matrices. Before describing these metrics in details, we stress that, while the median p -value of the 1D KS-tests has a clear statistical interpretation in terms hypothesis testing, and therefore allows to quantify the performances of a given model, the W-distance and the F-norm are distance measures, and cannot be interpreted as statistical tests.⁴ Therefore, these metrics only allow one to compare models with each others and to conclude when a model “is better” than another one, but do not allow one to draw conclusions on how “good” a model is or how much a model is better than another one.

- **The Kolmogorov-Smirnov test** is a statistical test used to determine whether or not two 1D samples come from the same *unknown* PDF. The null hypothesis assumes that both samples come from the same PDF. The KS statistic is given by

$$D_{y,z} = \sup_x |F_y(x) - F_z(x)| \quad (25)$$

where $F_{y,z}(x)$ are the empirical distributions of each of the samples $\{y_i\}$ and $\{z_i\}$, and \sup is the supremum function. The p -value for

rejecting the null-hypothesis is obtained as the maximal p satisfying the condition

$$D_{y,z} > \sqrt{-\ln\left(\frac{p}{2}\right) \cdot \frac{1 + \frac{n_z}{n_y}}{2n_z}}, \quad (26)$$

where n_y and n_z are the sizes of the two samples.

For characterizing the performances of our results, we compute the mean of the KS-test p -values obtained comparing several pairs of sub-samples of each 1D marginal distribution obtained from the test and NF generated samples. Then, we compute the median of the result for each dimension over all dimensions.

Since, under the null hypothesis, the p -value is a random variable with a uniform distribution in the $[0, 1]$ interval, and its mean and median are therefore equal to 0.5, which represents the optimal value for our test. We choose the median in place of the mean over dimensions to avoid, especially for very large dimensionality, that a few badly-performing dimensions could deliver a very small mean, leading to a too pessimistic interpretation of the performances. Nevertheless, we always also compute the mean over dimensions and observe good agreement with the median, signaling that, on average, all dimensions are learned “equally well”.

- **The Wasserstein distance** between two 1D distributions is given as a function of their respective empirical distributions as

$$W_{y,z} = \int_{\mathbb{R}} dx |F_y(x) - F_z(x)|. \quad (27)$$

Again, we compute the measure for each dimension and take the median over all dimensions and use it as our metric, whose optimal value is zero. In the following we refer to this metric simply as W-distance.

- **The Frobenius norm** of a matrix M is given by

$$M_F = \sqrt{\sum_{i,j} |m_{ij}|^2}, \quad (28)$$

where m_{ij} are the elements of M . By defining $M = C_y - C_z$, where $C_{y,z}$ are the correlation matrices of two distributions Y and Z of equal

⁴One could obviously define a test statistic based on these distances. However, the test statistic distribution would not be known a priori and hypothesis testing would require to perform pseudo-experiments. This is beyond the scope of our analysis.

dimensionality, we obtain a metric of the discrepancy between the correlation matrices of the two as

$$M_F = \sqrt{\sum_{i,j} |y_{ij} - z_{ij}|^2}, \quad (29)$$

where y_{ij} and z_{ij} are the elements of C_y and C_z , respectively. Notice that, since the F-norm tends to become larger as the size of the matrix increases, this metric, differently from the previous ones, depends on the dimensionality. Nonetheless, the optimal value is always zero.

5 Testing the Normalizing Flows

We tested the four architectures discussed above on three classes of toy distributions of various dimensionality: Correlated Mixture of Gaussians (CMoG), extremely multi-modal Correlated Mixture of Gaussians (CMoGem), and Truncated Distributions (TD). We describe them in turn in the following subsections.

In all cases we consider a training sample size of 10^5 with 70% used as training data and 30% used as validation data. The test sample size is always 10^5 .

5.1 Correlated Mixture of Gaussians

Our CMoG distributions are defined as follows: we take a mixture of $n = 3$ components $N = 4, 8, 16, 32, 64, 100, 200, 400, 1000$ dimensional multivariate Gaussian distributions with diagonal covariance matrices, defined by means randomly generated in the $[0, 10]$ interval and standard deviations randomly generated in the $[0, 1]$ interval⁵. The components are mixed according to an n dimensional categorical distribution (with random probabilities). This means that a different probability is assigned to each component, while different dimensions of the same component multivariate Gaussian are assigned the

same probability. The resulting multivariate distribution has random (order one) off-diagonal elements in the covariance matrix and multi-modal 1D marginal distributions.

For each of the four different algorithms described above and for each value of N we perform a small scan over some of the free hyperparameters. Details on the choice of the hyperparameters are reported in Appendix B. All models have been trained on Tesla V100 Nvidia GPUs.

The performances of the best NF models for the CMoG distributions are reported in Fig. 1 and Table 2. The figure shows the median 1D W-distance (upper-left), the median KS-test p -value (upper-right), the Frobenius norm (lower-left), and the training time (lower-right).⁶ The best models are chosen as those with the minimal median 1D W-distance. One could define the best models differently, for instance considering the median KS-test p -values, but the conclusions do not change substantially, since all metrics are rather correlated.

From Fig. 1 we immediately notice that the C-RQS algorithm does not converge above 100 dimensions, while the best compromise between low 1D W-distance, large median KS-test p -value, and small training time, is given by the A-RQS algorithm. Nevertheless, we see that for all points in the plots but the MAF in 1000 dimensions, the median KS-test p -values are above 0.2, which, considering the small training set size, can be considered a good result. Also training times are good, almost constant with respect to dimensionality (suggesting that they depend more on the training sample size than on the dimensionality of the target distribution), being often below one hour and never above a few hours. To give a pictorial idea of the A-RQS performances, in Fig. 4 we show the 1D and 2D marginal distributions for the $N = 1000$ dimensional CMoG for a selection of dimensions. This model produced a median KS-test p -value of 0.51 training with only 10^5 points for about 4 hours. Another example of the A-RQS performances is given by the best model in $N = 200$ dimensions, where we obtained a median KS-test p -value of 0.52 training for less than half an hour.

⁵The values for the means and standard deviations are chosen so that the different components can generally be resolved.

⁶There is a certain degree of uncertainty in the mentioned training times, which are slightly conservative. We had at our disposal two Tesla V100 GPUs and all models have been trained in pairs. This slightly decreased the performances of each single training, but improved the overall training time.

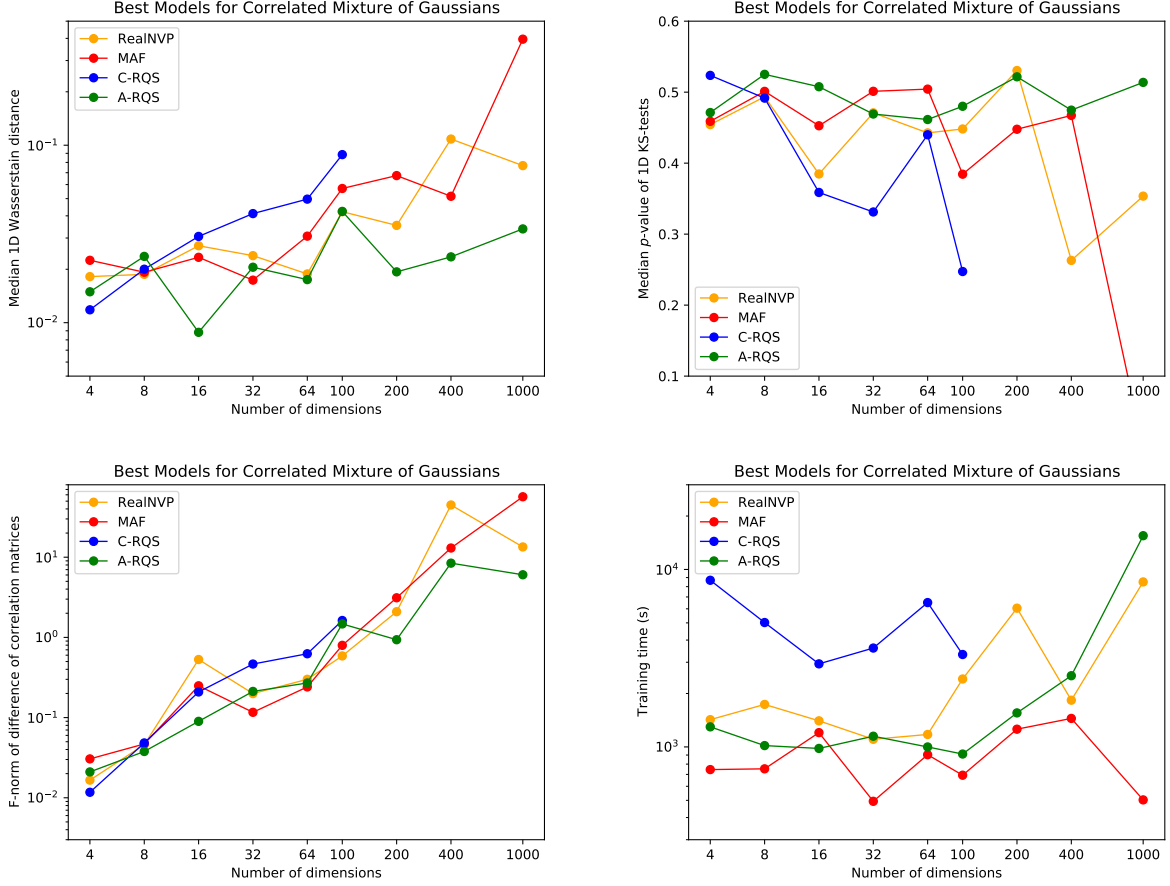


Fig. 1 Performance comparison between the best models obtained with RealNVP, MAF, C-RQS, and A-RQS architectures when learning the CMoG distributions, measured by the median 1D W-distance (upper-left), the median p -value of 1D KS-tests (upper-right), the F-norm of the difference between the correlation matrices (lower-left), and the training time (lower-right).

5.2 Extremely multi-modal CMoG

To push even further the complication of the target distribution, we generalized the CMoG to $n = 10$ components, where each component cannot be generally resolved anymore. We call this extremely multi-modal generalization CMoGem. We limited to 10 components to avoid data to look just as random noise. In this case we did not repeat the entire hyperparameters scan performed for the CMoG, but directly focused on the hyperparameters that ended up as best choices in the CMoG case. This also gives an idea of the generalization capabilities of the various algorithms. We also limited to $N \leq 400$ dimensions, since training became unstable for $N = 1000$ dimensions.

Results are shown in Fig. 2 and Table 3 and are similar to those of the CMoG case: the C-RQS algorithm does not converge above 100 dimensions and turns out to be the slowest algorithm. MAF and RealNVP generally perform well, with a slight preference for the MAF, which is also faster. The A-RQS algorithm performs well up to 100 dimensions, but performances deprecate for larger dimensionality. This also happens for MAF and RealNVP, even though in a less dramatic way. In order to check if the architecture for the A-RQS was too simple to generalize to the CMoGem case, we made two additional runs for the A-RQS with three layers with 512 nodes and 16 and 32 spline knots. The best models arising from this last run are shown in the figure as A-RQS 2 (dashed line). The improvement in performances, especially for

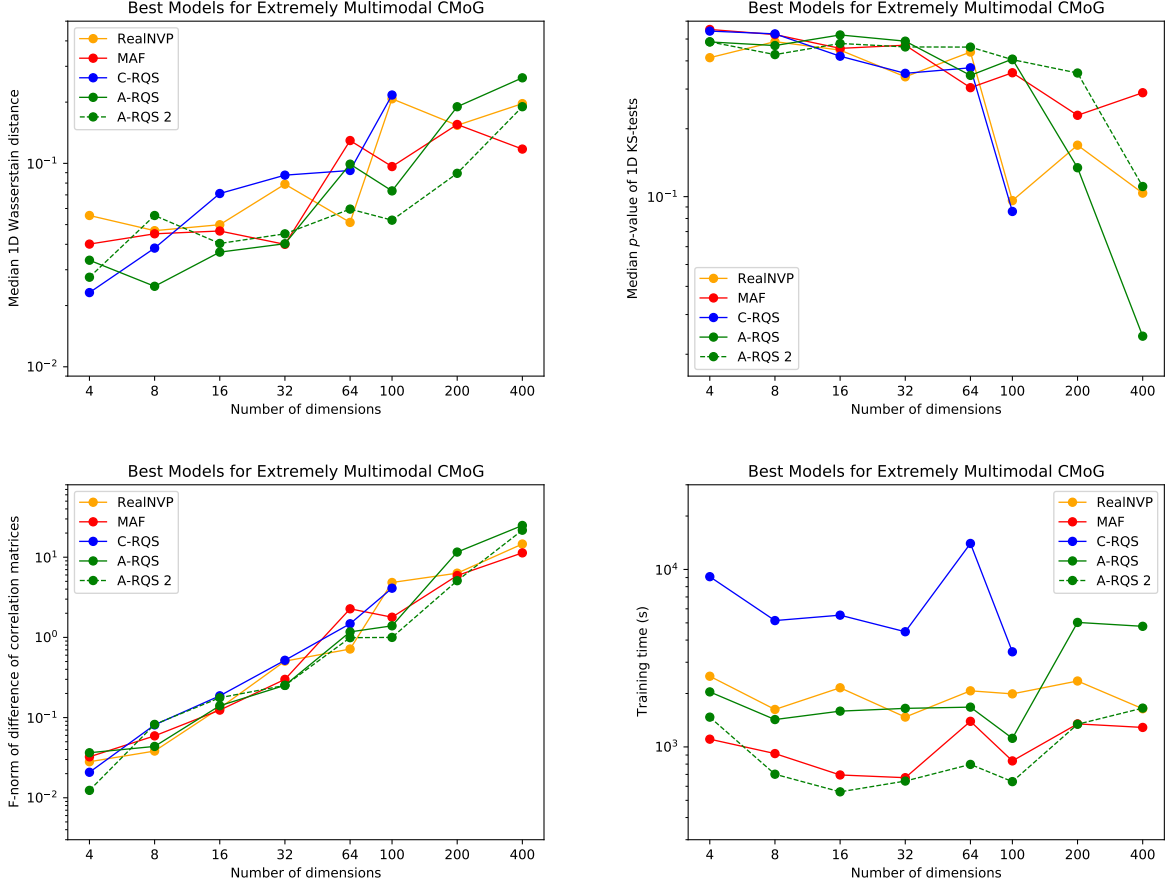


Fig. 2 Performance comparison between the best models obtained with RealNVP, MAF, C-RQS and A-RQS architectures when learning the CMoGem distributions, measured by the median 1D W-distance (upper-left), the median p -value of 1D KS-tests (upper-right), the F-norm of the difference between the correlation matrices (lower-left), and the training time (lower-right).

large dimensionality, is evident, and even more evident is the improvement in the training time, due to the smaller number of epochs needed for reaching the required convergence. Nevertheless, the MAF seems to be more stable in this case for dimensionality higher than 100 and still provides good training times. For comparison, also in this case we show, in Figure 5 the 1D and 2D marginal distributions for the $N = 200$ dimensional CMoGem for a selection of dimensions obtained with the best A-RQS 2 model. This model produced a median KS-test p -value of 0.35 training with only 10^5 points for about 22 minutes.

5.3 Truncated Gaussians

Normalizing Flows deliver, by construction, continuous distributions. In physics, it often happens to have distributions that are truncated, because of some kinematical or theoretical limit. It is therefore interesting to study how well our NF architectures can describe this type of distributions. To do so, we considered a class of distributions, that we call Truncated Gaussians (TG). For this case we consider dimensionalities up to $N = 100$ and mix uni-modal Gaussian distributions defined by means randomly generated in the $[0, 10]$ interval, standard deviations randomly generated in the $[0, 1]$ interval, and truncation implemented as follows: for each dimension we choose randomly between low, high, or two-side truncation and truncate on the mean for the first two cases and

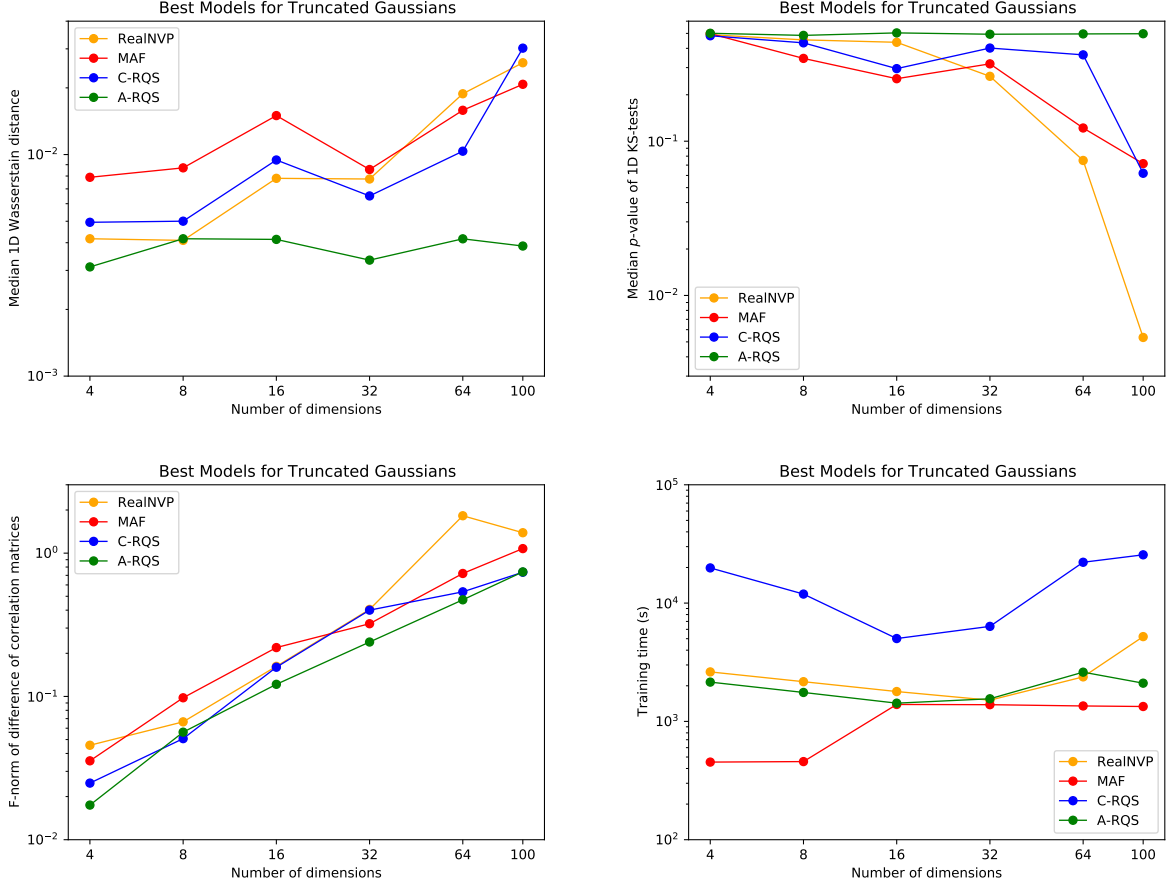


Fig. 3 Performance comparison between the best models obtained with RealNVP, MAF, C-RQS and A-RQS architectures when learning the TG distributions, measured by the median 1D W-distance (upper-left), the median p -value of 1D KS-tests (upper-right), the F-norm of the difference between the correlation matrices (lower-left), and the training time (lower-right).

between the mean minus one standard deviation and the mean plus one standard deviation for the last case. The resulting multivariate distribution is uncorrelated, i.e. has negligible off-diagonal terms in the correlation matrix.

Since our NF distributions are always defined over infinite continuous ranges, we transformed them with a soft clipping bijector with hinge 10^{-4} after training to ensure definite boundaries.⁷ A poorly modeled distribution beyond the boundaries would present large spikes at such limits after clipping. As before, a small hyperparameter scan

⁷The hinge represents the “smoothness” of the truncation, which is implemented, in the clipping bijector, as a differentiable function.

was performed to train the NFs. The hyperparameter space is the same as in the CMoG, and is shown in Table 1.

The best-performance configurations along with their corresponding metrics results for each flow architecture are shown in Fig. 3 and Table 4. Results are similar to those obtained for CMoG and CMoGem, with the exception of C-RQS, which remains the slowest architecture, but features better performances. Again the A-RQS proves to be the best choice in terms of both precision, timing, and scalability. For a visual representation of the performances we show, in Figure 6, the 1D and 2D marginal distributions for the $N = 100$ dimensional TG distribution for a selection of dimensions obtained with the best A-RQS model. This model produced a median KS-test p -value of about 0.5 training with only 10^5 points for

about 35 minutes. From the 1D marginal distributions in Fig. 6 one notices that, for a couple of dimensions, the NF tends to interpret as bi-modal the uni-modal distributions. While precision is very high in average, we believe that more precision in each of the dimensions may require more training points or a more fine-tuned model.

As a final remark, we would like to stress that performances of the architectures considered in this paper are expected to be sub-optimal when applied to fully uncorrelated distributions: coupling and autoregressive flows use information from some dimensions to learn others and when dimensions are uncorrelated obtaining good accuracies is more challenging. This is also confirmed by other experiments we performed with uncorrelated mixtures of Gaussians, which systematically resulted in poorer results than those obtained with CMoG of the same dimensionality. We believe that in case of uncorrelated distributions, other approaches need to be employed. Nevertheless, we do not consider fully uncorrelated distributions as a realistic example of HEP distributions since in those cases, at least for subsets of the dimensions, correlations are to be expected.

6 Conclusions and Outlook

Normalizing Flows have many potential applications in HEP, both in their normalizing and generative directions. However, to ensure a standardized usage and to match the required precision, their application to high-dimension datasets need to be properly evaluated. This paper makes a step forward in this direction by quantifying the ability of state-of-the-art coupling and autoregressive flow architectures to model distributions of increasing complexity and dimensionality. This was done by testing the most widely used brand of NFs in HEP, the coupling (RealNVP and C-RQS) and the autoregressive flows (MAF and A-RQS), against several classes of generic distributions. Performances were measured by means of different metrics and by considering the training times. As the main highlight, we found that the A-RQS is greatly capable of precisely learning all the high-dimensional complex distributions it was tested against, always within a few hours of training on a Tesla V100 GPU and with limited training data. As of the other tested architectures, our results show that reasonably good results can be obtained

with all of them but the C-RQS, which ended up being less stable and longer to train, especially in high dimensionality.

Our analysis was performed implementing all architectures in TENSORFLOW2 with TENSORFLOW PROBABILITY using PYTHON. The code is available in Ref. [56], while a general-purpose user-friendly framework for NFs in TensorFlow2 named NF4HEP is under development and can be found in Ref. [57].

We stress that the intention of this study is to secure generic assessments of how NFs perform in high dimensions. For this reason the target distributions were chosen independently of any particular experimentally-driven physics dataset. Nonetheless, this study represents the first of a series to come. Let us briefly mention, in turn, the research directions we aim to follow starting from the present paper.

- Development of reliable multivariate quality metrics, including approaches based on machine learning [58, 59]. New results [60–62] suggests that classifier-based two-sample tests have the potential to match the needs of the HEP community when paired with a careful statistical analysis. These tests can leverage different ML models to provide high flexibility and sensitivity together with short training times, especially when based on kernel methods [62]. On the other hand, further studies are needed to investigate their efficiency and scalability to high dimensions.
- Study of the dependence of the NF performances on the number of samples [63]. In the present paper we always kept the number of samples to 10^5 (70% used for training and 30% used for validation). It is clear that such number is pretty large in small dimensionality, like $N = 4$ dimensions, and undersized for large dimensionality, like $N \geq 100$. It is important to study the performances of the considered NF architectures in the case of scarce or very abundant data, assessing the dependency of the final precision on the number of training samples. This can also be related to developing techniques to infer the uncertainty of the NF models.
- An open question, particularly important for HEP applications, is whether generative models can be used for statistical augmentation, i.e. to generate more samples than those used for

training to reduce statistical uncertainty, or if uncertainty is dominated by the training sample size. Normalizing Flows, being semi-analytical generative models based on bijective maps, may be a good candidate class of models to assess the statistical augmentation properties. Indeed this essentially depends on how well the generative model learns the proper target distribution parameters: when the target distribution is learned parametrically, it is not unreasonable to expect good statistical augmentation performances. Nevertheless, in case statistical augmentation would prove to be poor in the generative direction, one could still use NF in the normalizing direction to build effective priors and proposals to enhance known sampling techniques, such as Markov Chain Monte Carlo, whose statistical properties are well known.

- Applications of the architectures and implementations developed in this project to real-data HEP cases are already under investigation. In a forthcoming publication we show how a $\mathcal{O}(100)$ dimensional experimental likelihood, arising from HEP global fits, can be efficiently learned by NFs.
- A final issue that needs to be addressed to ensure a widespread use of NFs in HEP is the ability to preserve and distribute pre-trained NF-based models. This is, for the time being, not an easy and standard task and support from the relevant software developer community will have to come to achieve this goal.

Acknowledgments

We thank Luca Silvestrini for pushing us towards the study of NFs and for fruitful discussions. We are thankful to the developers of TENSORFLOW2, which made possible to perform this analysis. We thank the IT team of INFN Genova, and in particular Mirko Corosu, for useful support. We are thankful to OpenAI for the development of ChatGPT and to ChatGPT itself for useful discussions. H.R.G. acknowledges the hospitality of Sabine Kraml at LPSC Grenoble and the discussions on Normalizing Flows held there with the rest of the SModelS Collaboration. This work was partially supported by the Italian PRIN grant 20172LNEEZ. M.L. acknowledges the financial support of the European Research Council (grant SLING 819789).

A Implementation of NF architectures

A.1 The RealNVP

We are given a collection of vectors $\{y_i^I\}$ with $i = 1, \dots, D$ representing the dimensionality and $I = 1, \dots, N$ the number of samples representing the unknown PDF p_Y . For all samples \mathbf{y}^I we consider the half partitioning given by the two sets $\hat{\mathbf{y}}^I = \{y_1^I, \dots, y_{D/2}^I\}$ and $\tilde{\mathbf{y}}^I = \{y_{D/2+1}^I, \dots, y_D^I\}$. We then use the $\hat{\mathbf{y}}^I$ samples as inputs to train a fully connected MLP (a dense DNN) giving as output the vectors of t_i and s_i , with $i = 1, \dots, D/2$ in Eq. (10). These output vectors are provided by the DNN through two output layers, which are dense layers with linear and tanh activation functions for t_i and s_i , respectively, and are used to implement the transformation in Eq. (12), which outputs the (inversely) transformed samples. Moreover, in order to transform all dimensions and to increase the expressivity of the model, we use a series of such RealNVP bijectors, feeding the output of each bijector as input for the next one, and inverting the role of the two partitions at each step. After the full transformation is performed, one obtains the final $\{x_i^I\}$ with $i = 1, \dots, D$ vectors and the transformation Jacobian (the product of the inverse of Eq. (11) for each bijector). With these ingredients, and assuming a normal base distribution p_X , one can compute the negative of the log-Likelihood of Eq. (2), which is used as loss function for the DNN optimization.

As it is clear from the implementation, the RealNVP Normalizing Flow, i.e. the series of RealNVP bijectors, is trained in the normalizing direction, taking data samples as inputs. Nevertheless, since the s_i and t_i vectors only depend, at each step, on untransformed dimensions, once the DNN is trained, they can be used both to compute the density, by using Eq. (12) and to generate new samples, with equal efficiency, by using Eq. (10). This shows that the RealNVP is equally efficient in both the normalizing and generative directions.

A.2 The MAF

As in the case of the RealNVP, also for the MAF, the forward direction represents the normalizing direction. In this case the vectors s_i and t_i , of dimension $D - 1$ describing the affine bijector

in Eq. (13) are parametrized by an autoregressive DNN with D inputs and $2(D - 1)$ outputs, implemented through the MADE [54] masking procedure, according to the TensorFlow Probability implementation (see [64]). The procedure is based on binary mask matrices defining which connections (weights) are kept and which are dropped to ensure the autoregressive property.⁸ Mask matrices are determined from numbers (degrees) assigned to all nodes in the DNN: each node in the input layer is numbered sequentially from 1 to D ; each node in each hidden layer is assigned a number between 1 and D , possibly with repetition; the first half output nodes (representing s_i) are numbered sequentially from 1 to $D - 1$ and the same for the second half (representing t_i). Once all degrees are assigned, the matrix elements of the mask matrices are 1 if two nodes are connected and 0 if they are “masked”, i.e. not connected. The mask matrices are determined connecting the nodes of each layer with index k with all nodes in the preceding layer having an index smaller or equal than k . As for the RealNVP, a series of MAF bijectors is used, by feeding each with the $\{x_i^f\}$, with $i = 1, \dots, D$, according to Eq. (15) computed from the previous one. The last bijector computes the final $\{x_i^f\}$, with $i = 1, \dots, D$, according to Eq. (15) and the transformation Jacobian (the product of the inverse of Eq. (14) for each bijector), used to compute and optimize the log-Likelihood as defined in Eq. (2).

The efficiency of the MAF in the normalizing and generative directions is not the same, as in the case of the RealNVP. Indeed, computing the log-Likelihood for density estimation, requires a single forward pass of $\{y_i\}$ through the NF. However, generating samples requires to start from $\{x_i\}$, randomly generated from the base distribution. Then one needs the following procedure to compute the corresponding $\{y_i\}$:

- define the first component of the required y_i^{input} as $y_1^{\text{output}} = y_1^{\text{input}} = x_1$ where y_i^{input} is the NF input;
- start with a $y_i^{\text{input}} = x_i$ and pass it through the NF to determine y_2^{output} as function of y_1^{output} ;

- update y_i^{input} with $y_2^{\text{input}} = y_2^{\text{output}}$ and pass through the NF to determine y_3^{output} as function of y_1^{output} and y_2^{output} ;
- iterate until all the y_i^{output} components are computed.

It is clear to see that the procedure requires D passes through the NF to generate a sample, so that generation in the MAF is D times less efficient than density estimation. The Inverse Autoregressive Flow (IAF) [53] is an implementation similar to the MAF that implements generation in the forward direction (obtained by exchanging x and y in Eqs (13) and (15)). In the case of IAF, computing the log-Likelihood (which is needed for training) requires D steps, while generation only requires a single pass through the flow. The IAF is therefore much slower to train and much faster to generate new samples.

A.3 The C-RQS

The C-RQS parameters are determined by the following procedure [51].

1. A dense DNN takes x_1, \dots, x_d as inputs, and outputs an unconstrained parameter vector θ_i of length $3K - 1$ for each $i = d + 1, \dots, D$ dimension.
2. The vector θ_i is partitioned as $\theta_i = [\theta_i^w, \theta_i^h, \theta_i^d]$, where θ_i^w and θ_i^h have length K , while θ_i^d has length $K - 1$;
3. The vectors θ_i^w and θ_i^h are each passed through a softmax and multiplied by $2B$; the outputs are interpreted as the widths and heights of the K bins, which must be positive and span the \mathbb{B} interval. Then, the cumulative sums of the K bin widths and heights, each starting at $-B$, yield the $K + 1$ knots parameters $\{(x_i^{(k)}, y_i^{(k)})\}_{k=0}^K$;
4. The vector θ_i^d is passed through a softplus function and is interpreted as the values of the derivatives $\{d_i^{(k)}\}_{k=1}^{K-1}$ at the internal knots.

As for the RealNVP, in order to transform all dimensions, a series of RQS bijectors is applied, inverting the role of the two partitions at each step.

⁸The binary mask matrices are simple transition matrices between pairs of layers of dimension (K', K) with K' the number of nodes in the forward layer (closer to the output) and K the number of nodes in the backward layer (closer to the input). Obviously $K = D$ for the input layer and $K' = D$ for the output layer.

Hyperparameters for the MoG models				
Hyperpar.	MAF	RealNVP	A-RQS	C-RQS
number of bijectors	5, 10	5, 10	2	5, 10
number of hidden layers	3×128 3×256	3×128 3×256	3×128 3×256	3×128 3×256 3×512
number of spline knots	–	–	8, 12	8, 12
total number of runs	4	4	4	12

Table 1 Hyperparameter values used in our analysis.

A.4 The A-RQS

In the autoregressive implementation, we follow the same procedure used in the MAF implementation and described in Section A.2, but instead of obtaining the $2(D-1)$ outputs determining the affine parameters, we obtain the $3K-1$ parameters needed to compute the values of the knots parameters and derivatives. Once these are determined the procedure follows the steps 2 to 4 of the C-RQS implementation described in the previous subsection.

B Hyperparameters

For all models we used a total of 10^5 training (70% used for actual training and 30% used for validation) and 10^5 test points. We employed ReLU activation function with no regularization. All models were trained for up to 1000 epochs with initial learning rate set to 10^{-3} . The learning rate was reduced by a factor of 0.2 after 50 epochs without improvement better than 10^{-4} on the validation loss. Early stopping was used to terminate the learning after 60 epochs without the same amount of improvement. The batch size was set to 256 for RealNVP and to 512 for the other algorithms. For the two neural spline algorithms we also set the range of the spline equal to $[-16, 16]$. All other relevant hyperparameters, with their multiple values when they are scanned over, are reported in Table 1.

C Correlated mixture of Gaussians

Best models for CMoG									
hidden layers	# of bijec.	algorithm	spline knots	batch size	Median W-distance	Median KS-test	Frobenius Norm	# of epochs	training time (s)
4D									
3×128	5	C-RQS	8	512	1.18e-02	5.24e-01	1.17e-02	310	8690
3×256	2	A-RQS	12	512	1.49e-02	4.71e-01	2.10e-02	237	1297
3×128	5	RealNVP	–	256	1.82e-02	4.54e-01	1.66e-02	268	1424
3×128	5	MAF	–	512	2.25e-02	4.59e-01	3.05e-02	323	745
8D									
3×128	5	RealNVP	–	256	1.87e-02	4.93e-01	4.59e-02	325	1735
3×128	5	MAF	–	512	1.92e-02	5.01e-01	4.69e-02	327	752
3×128	5	C-RQS	12	512	2.00e-02	4.92e-01	4.83e-02	198	5022
3×128	2	A-RQS	12	512	2.36e-02	5.25e-01	3.78e-02	190	1017
16D									
3×128	2	A-RQS	8	512	8.82e-03	5.08e-01	8.98e-02	184	980
3×128	10	MAF	–	512	2.34e-02	4.53e-01	2.49e-01	153	1203
3×128	10	RealNVP	–	256	2.71e-02	3.85e-01	5.30e-01	147	1403
3×128	5	C-RQS	8	512	3.06e-02	3.59e-01	2.09e-01	148	2937
32D									
3×256	5	MAF	–	512	1.74e-02	5.01e-01	1.16e-01	176	493
3×128	2	A-RQS	8	512	2.05e-02	4.69e-01	2.12e-01	220	1148
3×128	5	RealNVP	–	256	2.39e-02	4.71e-01	1.99e-01	207	1104
3×128	5	C-RQS	12	512	4.12e-02	3.31e-01	4.65e-01	142	3606
64D									
3×128	2	A-RQS	8	512	1.75e-02	4.61e-01	2.70e-01	189	999
3×128	5	RealNVP	–	256	1.88e-02	4.43e-01	3.00e-01	245	1175
3×128	5	MAF	–	512	3.07e-02	5.04e-01	2.41e-01	317	903
3×128	5	C-RQS	12	512	4.97e-02	4.40e-01	6.25e-01	249	6506
100D									
3×128	5	RealNVP	–	256	4.22e-02	4.48e-01	5.87e-01	429	2414
3×256	2	A-RQS	12	512	4.24e-02	4.80e-01	1.47e+00	149	911
3×256	10	MAF	–	512	5.70e-02	3.84e-01	7.96e-01	141	692
3×512	5	C-RQS	8	512	8.85e-02	2.47e-01	1.62e+00	148	3317
200D									
3×128	2	A-RQS	12	512	1.93e-02	5.22e-01	9.35e-01	263	1554
3×256	10	RealNVP	–	256	3.53e-02	5.30e-01	2.09e+00	548	6051
3×128	5	MAF	8	512	6.74e-02	4.48e-01	3.12e+00	484	1258
400D									
3×128	2	A-RQS	8	512	2.35e-02	4.75e-01	8.43e+00	313	2518
3×128	5	MAF	–	512	5.16e-02	4.67e-01	1.30e+01	365	1447
3×256	10	RealNVP	–	256	1.08e-01	2.63e-01	4.48e+01	163	1833
1000D									
3×128	2	A-RQS	8	512	3.38e-02	5.14e-01	6.04e+00	1000	15493
3×128	10	RealNVP	–	256	7.67e-02	3.54e-01	1.34e+01	592	8504
3×128	5	MAF	–	512	3.96e-01	3.02e-05	5.67e+01	133	502

Table 2 Values of the most relevant hyperparameters and metrics for the best models in the case of the CMoG distributions. The number of training epochs and the training time are also shown, giving an idea of how much each model needs to be trained.

D Extremely multimodal correlated mixture of Gaussians

Best models for CMoGem									
hidden layers	# of bijec.	algorithm	spline knots	batch size	Median W-distance	Median KS-test	Frobenius Norm	# of epochs	training time (s)
4D									
3 × 128	5	C-RQS	8	512	2.32e-02	5.42e-01	2.08e-02	459	9105
3 × 512	2	A-RQS2	64	512	2.76e-02	4.86e-01	1.24e-02	275	1471
3 × 256	2	A-RQS	12	512	3.34e-02	4.85e-01	3.64e-02	361	2041
3 × 128	5	MAF	–	512	4.01e-02	5.51e-01	3.24e-02	446	1105
3 × 128	5	RealNVP	–	256	5.54e-02	4.13e-01	2.81e-02	453	2502
8D									
3 × 128	2	A-RQS	12	512	2.49e-02	4.68e-01	4.37e-02	255	1426
3 × 128	5	C-RQS	12	512	3.83e-02	5.27e-01	8.11e-02	213	5151
3 × 128	5	MAF	–	512	4.51e-02	5.23e-01	5.92e-02	368	917
3 × 128	5	RealNVP	–	256	4.67e-02	4.87e-01	3.83e-02	288	1625
3 × 512	2	A-RQS2	64	512	5.54e-02	4.27e-01	8.22e-02	127	701
16D									
3 × 128	2	A-RQS	8	512	3.66e-02	5.21e-01	1.41e-01	293	1590
3 × 512	2	A-RQS2	32	512	4.04e-02	4.78e-01	1.77e-01	101	558
3 × 256	10	MAF	–	512	4.65e-02	4.54e-01	1.24e-01	142	694
3 × 128	10	RealNVP	–	256	4.99e-02	4.47e-01	1.31e-01	205	2154
3 × 128	5	C-RQS	8	512	7.11e-02	4.20e-01	1.87e-01	262	5525
32D									
3 × 256	5	MAF	–	512	4.00e-02	4.69e-01	3.00e-01	261	670
3 × 128	2	A-RQS	8	512	4.03e-02	4.89e-01	2.53e-01	301	1648
3 × 512	2	A-RQS2	64	512	4.50e-02	4.61e-01	2.52e-01	110	642
3 × 128	5	RealNVP	–	256	7.90e-02	3.40e-01	5.06e-01	272	1473
3 × 128	5	C-RQS	12	512	8.75e-02	3.52e-01	5.18e-01	163	4456
64D									
3 × 128	5	RealNVP	–	256	5.13e-02	4.38e-01	7.16e-01	369	2070
3 × 512	2	A-RQS2	64	512	5.96e-02	4.60e-01	9.92e-01	116	797
3 × 128	5	C-RQS	12	512	9.23e-02	3.73e-01	1.48e+00	485	14009
3 × 128	2	A-RQS	8	512	9.91e-02	3.45e-01	1.17e+00	227	1675
3 × 128	5	MAF	–	512	1.29e-01	3.04e-01	2.27e+00	482	1393
100D									
3 × 512	2	A-RQS2	32	512	5.26e-02	4.05e-01	1.00e+00	95	637
3 × 256	2	A-RQS	12	512	7.32e-02	4.07e-01	1.39e+00	193	1118
3 × 256	10	MAF	–	512	9.64e-02	3.54e-01	1.78e+00	166	833
3 × 128	5	RealNVP	–	256	2.08e-01	9.60e-02	4.84e+00	383	1990
3 × 512	5	C-RQS	8	512	2.17e-01	8.60e-02	4.11e+00	144	3435
200D									
3 × 512	2	A-RQS2	64	512	8.93e-02	3.53e-01	5.10e+00	102	1342
3 × 256	10	RealNVP	–	256	1.54e-01	1.69e-01	6.32e+00	221	2351
3 × 128	5	MAF	–	512	1.55e-01	2.29e-01	5.91e+00	492	1348
3 × 128	2	A-RQS	12	512	1.90e-01	1.34e-01	1.16e+01	849	5030
400D									
3 × 128	5	MAF	–	512	1.18e-01	2.89e-01	1.13e+01	460	1287
3 × 512	2	A-RQS2	32	512	1.90e-01	1.11e-01	2.17e+01	116	1654
3 × 256	10	RealNVP	–	256	1.97e-01	1.04e-01	1.46e+01	152	1640
3 × 128	2	A-RQS	8	512	2.63e-01	2.41e-02	2.49e+01	701	4781

Table 3 Values of the most relevant hyperparameters and metrics for the best models in the case of the CMoGem distributions. The number of training epochs and the training time are also shown, giving an idea of how much each model needs to be trained.

E Truncated Gaussians

Best models for TG									
hidden layers	# of bijec.	algorithm	spline knots	batch size	Median W-distance	Median KS-test	Frobenius Norm	# of epochs	training time (s)
4D									
3×256	2	A-RQS	12	512	3.11e-03	5.01e-01	1.74e-02	389	2148
3×128	10	RealNVP	–	256	4.17e-03	4.90e-01	4.56e-02	248	2620
3×128	10	C-RQS	12	512	4.95e-03	4.83e-01	2.48e-02	340	19829
3×256	5	MAF	–	512	7.90e-03	4.98e-01	3.55e-02	188	452
8D									
3×128	10	RealNVP	–	256	4.10e-03	4.54e-01	6.65e-02	208	2166
3×128	2	A-RQS	12	512	4.17e-03	4.85e-01	5.63e-02	314	1756
3×512	10	C-RQS	8	512	5.00e-03	4.34e-01	5.07e-02	266	11918
3×128	5	MAF	–	512	8.71e-03	3.44e-01	9.78e-02	190	457
16D									
3×128	2	A-RQS	12	512	4.14e-03	5.04e-01	1.21e-01	259	1426
3×128	5	RealNVP	–	256	7.81e-03	4.38e-01	1.62e-01	360	1788
3×128	5	C-RQS	12	512	9.45e-03	2.95e-01	1.60e-01	196	5015
3×128	10	MAF	–	512	1.50e-02	2.54e-01	2.19e-01	304	1390
32D									
3×128	2	A-RQS	12	512	3.34e-03	4.94e-01	2.40e-01	295	1553
3×128	5	C-RQS	12	512	6.50e-03	4.02e-01	4.00e-01	255	6355
3×256	5	RealNVP	–	256	7.76e-03	2.63e-01	4.05e-01	343	1510
3×128	10	MAF	–	512	8.56e-03	3.17e-01	3.22e-01	307	1384
64D									
3×128	2	A-RQS	12	512	4.17e-03	4.96e-01	4.72e-01	350	2607
3×128	5	C-RQS	12	512	1.04e-02	3.63e-01	5.37e-01	932	22134
3×128	10	MAF	–	512	1.58e-02	1.22e-01	7.21e-01	324	1350
3×128	10	RealNVP	–	256	1.88e-02	7.50e-02	1.82e+00	260	2378
100D									
3×128	2	A-RQS	8	512	3.86e-03	4.97e-01	7.40e-01	384	2104
3×128	10	MAF	–	512	2.08e-02	7.15e-02	1.08e+00	304	1336
3×256	5	RealNVP	–	256	2.60e-02	5.34e-03	1.39e+00	1000	5208
3×256	5	C-RQS	12	512	3.02e-02	6.20e-02	7.36e-01	1000	25587

Table 4 Values of the most relevant hyperparameters and metrics for the best models in the case of the TG distributions. The number of training epochs and the training time are also shown, giving an idea of how much each model needs to be trained.

F Corner plots

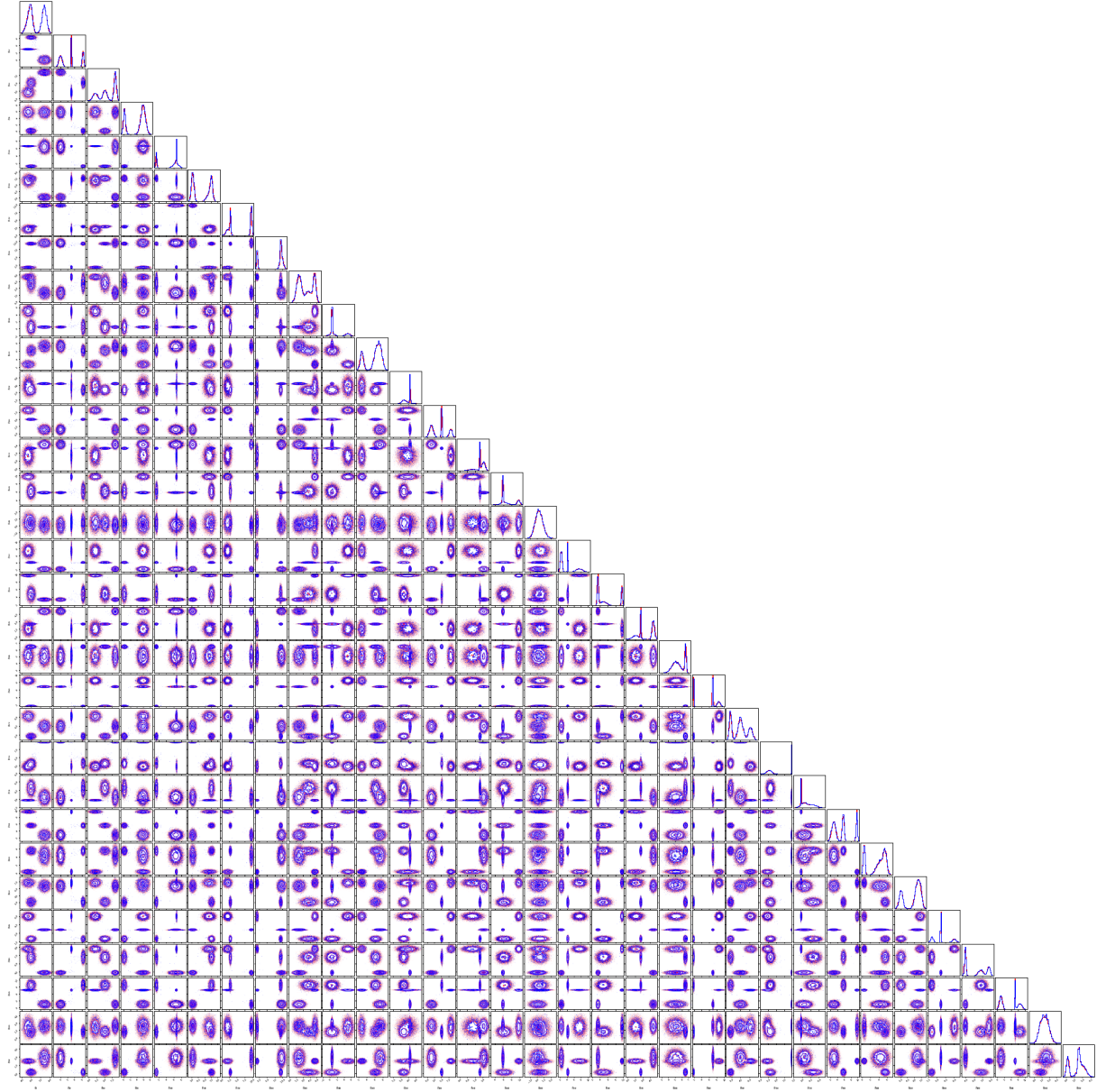


Fig. 4 1D and 2D marginal distributions for 32 randomly chosen dimensions of the $N = 1000$ dimensional CMoG distribution. Red and blue curves and points represent the test samples and the NF generated samples obtained with the A-RQS best model, respectively. Considering the high dimensionality, the non-trivial structure of the distribution, the limited number of training samples, and the low level of tuning of the hyperparameters, the result can be considered very accurate.

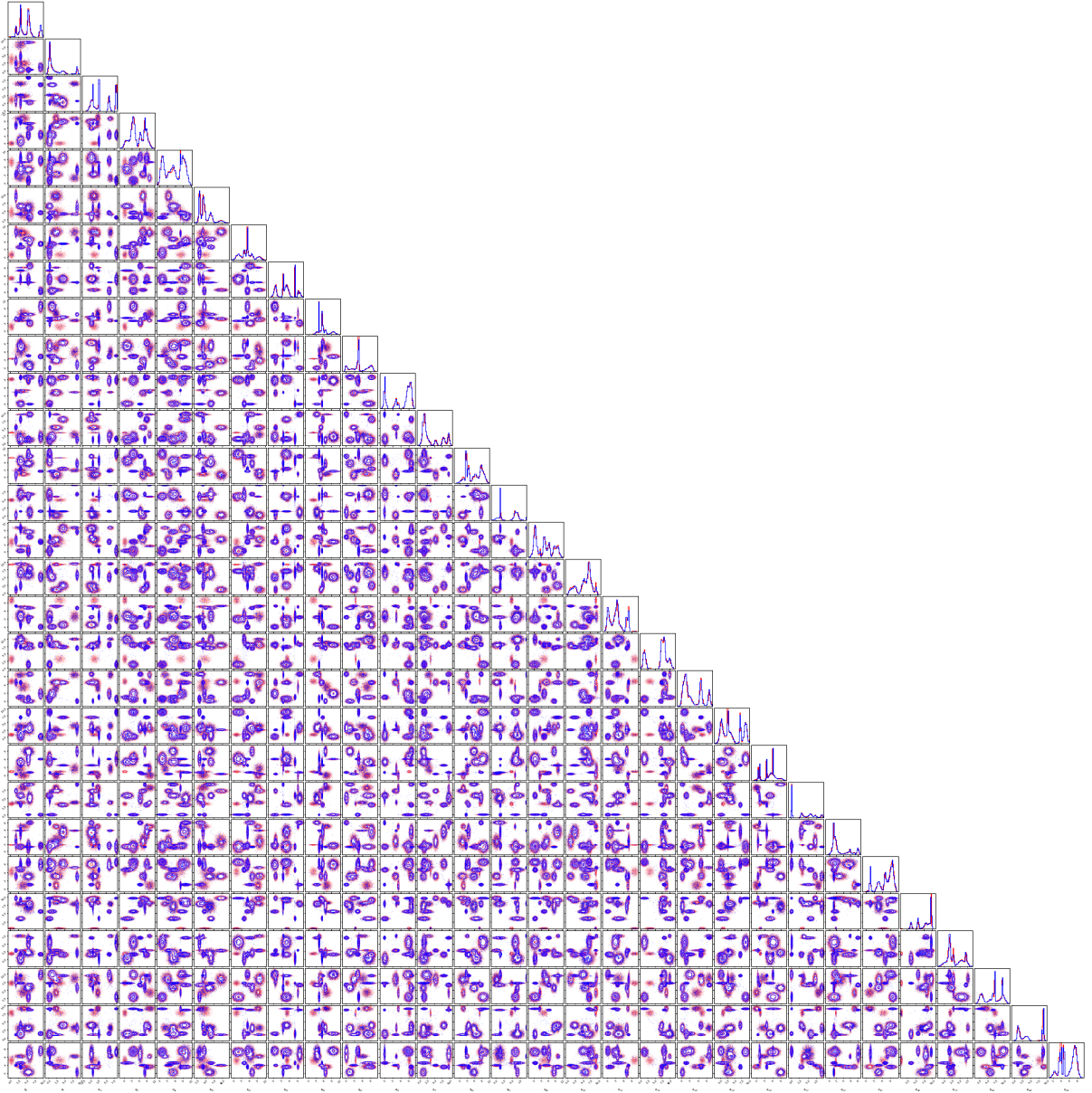


Fig. 5 1D and 2D marginal distributions for 29 randomly chosen dimensions of the $N = 200$ dimensional CMoGem distribution. Red and blue curves and points represent the test samples and the NF generated samples obtained with the A-RQS 2 best model, respectively. Considering the high dimensionality, the non-trivial structure of the distribution, the limited number of training samples, and the low level of tuning of the hyperparameters, the result can be considered very accurate.

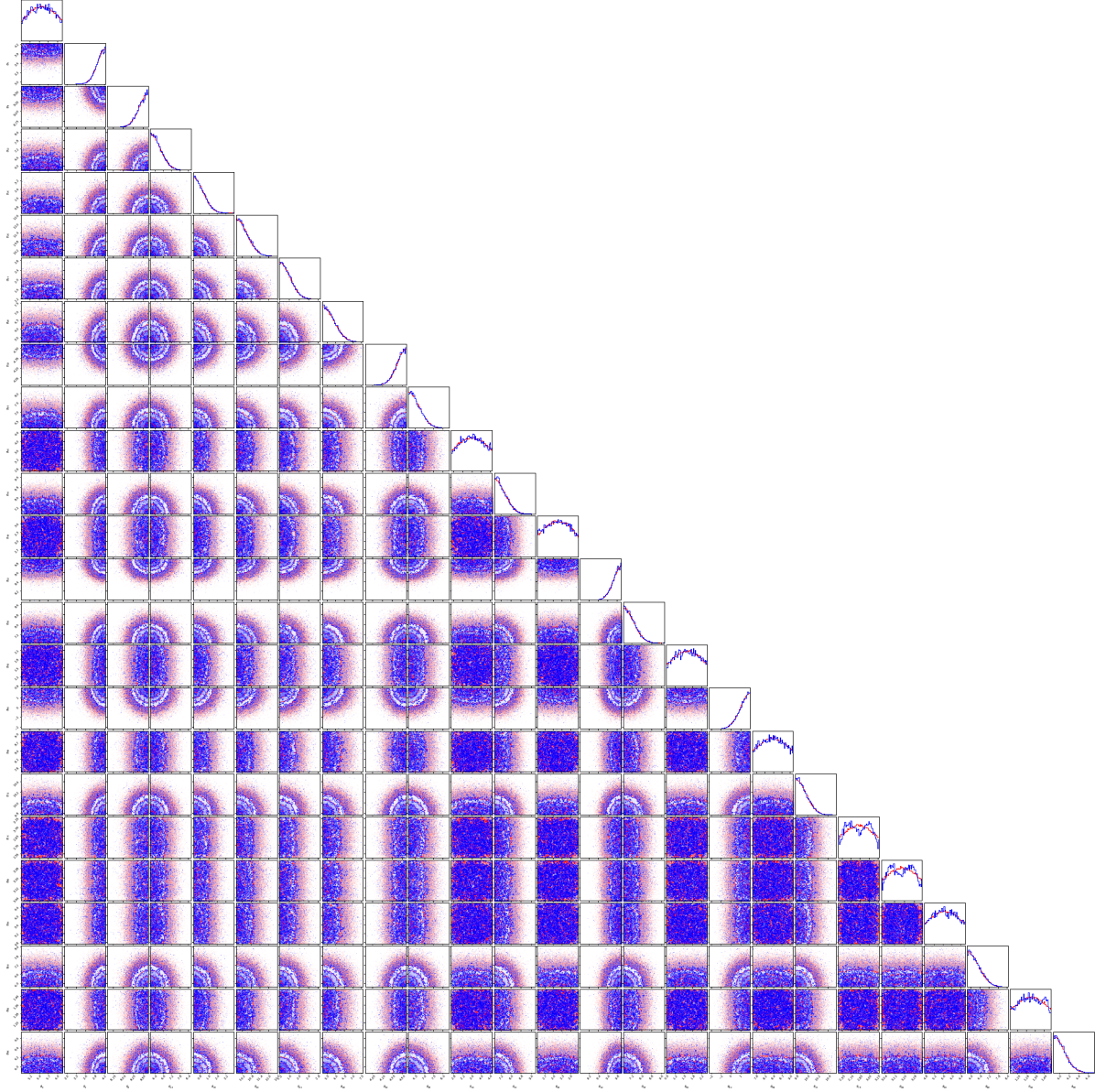




Fig. 6 1D and 2D marginal distributions for 25 randomly chosen dimensions of the $N = 100$ dimensional TG distribution. Red and blue curves and points represent the test samples and the NF generated samples obtained with the A-RQS best model, respectively. Considering the high dimensionality, the non-trivial structure of the distribution, the limited number of training samples, and the low level of tuning of the hyperparameters, the result can be considered very accurate.

References

- [1] [INSPIREHEP Search Results](#).
- [2] M. Feickert and B. Nachman, “A *Living Review of Machine Learning for Particle Physics*”, [arXiv:2102.02770](#) [[SEMANTIC SCHOLAR](#)].
- [3] K. Albertsson, P. Altoe, D. Anderson, M. Andrews, J. P. A. Espinosa, A. Aurisano et al., “*Machine Learning in High Energy Physics Community White Paper*”, *Journal of Physics: Conference Series* **1085** (2018) 022008, [arXiv:1807.02876](#) [[SEMANTIC SCHOLAR](#)].
- [4] P. Shanahan et al., “*Snowmass 2021 Computational Frontier CompF03 Topical Group Report: Machine Learning*”, [arXiv:2209.07559](#) [[SEMANTIC SCHOLAR](#)].
- [5] D. Bourilkov, “*Machine and Deep Learning Applications in Particle Physics*”, *Int. J. Mod. Phys. A* **34** (2020) 1930019, [arXiv:1912.08245](#) [[SEMANTIC SCHOLAR](#)].
- [6] G. Karagiorgi, G. Kasieczka, S. Kravitz, B. Nachman and D. Shih, “*Machine Learning in the Search for New Fundamental Physics*”, *Nature Rev. Phys.* **4** (2022) 399, [arXiv:2112.03769](#) [[SEMANTIC SCHOLAR](#)].
- [7] E. Tabak and E. Vanden-Eijnden, “*Density estimation by dual ascent of the log-likelihood*”, *Communications in Mathematical Sciences* **8** (2010) 217 [[SEMANTIC SCHOLAR](#)].
- [8] E. Tabak and C. Turner, “*A family of non-parametric density estimation algorithms*”, *Communications on Pure and Applied Mathematics* **66** (2013) 145 [[SEMANTIC SCHOLAR](#)].
- [9] D. J. Rezende and S. Mohamed, “*Variational Inference with Normalizing Flows*”, in *International Conference on Machine Learning*, 2015, [arXiv:1505.05770](#) [[SEMANTIC SCHOLAR](#)].
- [10] L. Dinh, D. Krueger and Y. Bengio, “*NICE: Non-linear Independent Components Estimation*”, [arXiv:1410.8516](#) [[SEMANTIC SCHOLAR](#)].
- [11] I. Goodfellow, J. Pouget-Abadie, M. Mirza, B. Xu, D. Warde-Farley, S. Ozair et al., “*Generative Adversarial Nets*”, in *Advances in Neural Information Processing Systems*, Z. Ghahramani, M. Welling, C. Cortes, N. Lawrence and K. Weinberger, eds., vol. 27, Curran Associates, Inc., 2014, [arXiv:1406.2661](#) [[SEMANTIC SCHOLAR](#)].
- [12] D. P. Kingma and M. Welling, “*Auto-Encoding Variational Bayes*”, in *2nd International Conference on Learning Representations, ICLR 2014, Banff, AB, Canada, April 14-16, 2014, Conference Track Proceedings*, 2014, [arXiv:1312.6114](#) [[SEMANTIC SCHOLAR](#)].
- [13] D. J. Rezende, S. Mohamed and D. Wierstra, “*Stochastic Backpropagation and Approximate Inference in Deep Generative Models*”, in *Proceedings of the 31st International Conference on Machine Learning*, E. P. Xing and T. Jebara, eds., vol. 32 of *Proceedings of Machine Learning Research*, pp. 1278–1286, PMLR, Beijing, China, 22–24 jun, 2014, [arXiv:1401.4082](#) [[SEMANTIC SCHOLAR](#)].
- [14] Y. Fan, D. J. Nott and S. A. Sisson, “*Approximate Bayesian computation via regression density estimation*”, *Stat* **2** (2013) 34, [arXiv:1212.1479](#) [[SEMANTIC SCHOLAR](#)].
- [15] G. Papamakarios and I. Murray, “*Fast ϵ -free Inference of Simulation Models with Bayesian Conditional Density Estimation*”, in *Advances in Neural Information Processing Systems*, D. Lee, M. Sugiyama, U. Luxburg, I. Guyon and R. Garnett, eds., vol. 29, Curran Associates, Inc., 2016, [arXiv:1605.06376](#) [[SEMANTIC SCHOLAR](#)].
- [16] J. Brehmer, G. Louppe, J. Pavez and K. Cranmer, “*Mining gold from implicit models to improve likelihood-free inference*”, *Proc. Nat. Acad. Sci.* **117** (2020) 5242, [arXiv:1805.12244](#) [[SEMANTIC SCHOLAR](#)].
- [17] S. R. Green, C. Simpson and J. Gair, “*Gravitational-wave parameter estimation with autoregressive neural network*

- flows”, *Phys. Rev. D* **102** (2020) 104057, [arXiv:2002.07656](#) [SEMANTIC SCHOLAR].
- [18] V. A. Villar, “Amortized Bayesian Inference for Supernovae in the Era of the Vera Rubin Observatory Using Normalizing Flows”, in *36th Conference on Neural Information Processing Systems*, 11, 2022, [arXiv:2211.04480](#) [SEMANTIC SCHOLAR].
- [19] J.-E. Campagne, F. Lanusse, J. Zuntz, A. Boucaud, S. Casas, M. Karamanis et al., “JAX-COSMO: An End-to-End Differentiable and GPU Accelerated Cosmology Library”, [arXiv:2302.05163](#) [SEMANTIC SCHOLAR].
- [20] M. Bellagente, “Go with the Flow: Normalising Flows applications for High Energy Physics”, *PhD Thesis, U. Heidelberg* (2022) [SEMANTIC SCHOLAR].
- [21] D. Zoran and Y. Weiss, “From learning models of natural image patches to whole image restoration”, in *Proceedings of the 13rd International Conference on Computer Vision*, pp. 479–486, 2011 [SEMANTIC SCHOLAR].
- [22] S. R. Green and J. Gair, “Complete parameter inference for GW150914 using deep learning”, *Mach. Learn. Sci. Tech.* **2** (2021) 03LT01, [arXiv:2008.03312](#) [SEMANTIC SCHOLAR].
- [23] T. Glüsenkamp, “Unifying supervised learning and VAEs – automating statistical inference in (astro-)particle physics with amortized conditional normalizing flows”, [arXiv:2008.05825](#) [SEMANTIC SCHOLAR].
- [24] D. Kodi Ramanah, R. Wojtak, Z. Ansari, C. Gall and J. Hjorth, “Dynamical mass inference of galaxy clusters with neural flows”, *Mon. Not. Roy. Astron. Soc.* **499** (2020) 1985, [arXiv:2003.05951](#) [SEMANTIC SCHOLAR].
- [25] D. H. T. Cheung, K. W. K. Wong, O. A. Hannuksela, T. G. F. Li and S. Ho, “Testing the robustness of simulation-based gravitational-wave population inference”, *Phys. Rev. D* **106** (2022) 083014, [arXiv:2112.06707](#) [SEMANTIC SCHOLAR].
- [26] D. Ruhe, K. Wong, M. Cranmer and P. Forré, “Normalizing Flows for Hierarchical Bayesian Analysis: A Gravitational Wave Population Study”, [arXiv:2211.09008](#) [SEMANTIC SCHOLAR].
- [27] S. S. Gu, Z. Ghahramani and R. E. Turner, “Neural Adaptive Sequential Monte Carlo”, in *Advances in Neural Information Processing Systems*, C. Cortes, N. Lawrence, D. Lee, M. Sugiyama and R. Garnett, eds., vol. 28, Curran Associates, Inc., 2015, [arXiv:1506.03338](#) [SEMANTIC SCHOLAR].
- [28] B. Paige and F. Wood, “Inference Networks for Sequential Monte Carlo in Graphical Models”, in *Proceedings of the 33rd International Conference on International Conference on Machine Learning - Volume 48*, ICML’16, p. 3040–3049, JMLR.org, 2016, [arXiv:1602.06701](#) [SEMANTIC SCHOLAR].
- [29] S. Foreman, T. Izubuchi, L. Jin, X.-Y. Jin, J. C. Osborn and A. Tomiya, “HMC with Normalizing Flows”, *PoS LATTICE2021* (2022) 073, [arXiv:2112.01586](#) [SEMANTIC SCHOLAR].
- [30] A. Singha, D. Chakrabarti and V. Arora, “Conditional normalizing flow for Markov chain Monte Carlo sampling in the critical region of lattice field theory”, *Phys. Rev. D* **107** (2023) 014512 [SEMANTIC SCHOLAR].
- [31] M. Caselle, E. Cellini, A. Nada and M. Panero, “Stochastic normalizing flows for lattice field theory”, *PoS LATTICE2022* (2023) 005, [arXiv:2210.03139](#) [SEMANTIC SCHOLAR].
- [32] A. G. D. G. Matthews, M. Arbel, D. J. Rezende and A. Doucet, “Continual Repeated Annealed Flow Transport Monte Carlo”, in *International Conference on Machine Learning*, 1, 2022, [arXiv:2201.13117](#) [SEMANTIC SCHOLAR].

- [33] G. Papamakarios and I. Murray, “*Distilling Intractable Generative Models*”, in *Probabilistic Integration Workshop at the Neural Information Processing Systems Conference, 2015*, 2015 [SEMANTIC SCHOLAR].
- [34] M. Gabri  , G. M. Rotskoff and E. Vanden-Eijnden, “*Adaptive Monte Carlo augmented with normalizing flows*”, *Proc. Nat. Acad. Sci.* **119** (2022) e2109420119, [arXiv:2105.12603](#) [SEMANTIC SCHOLAR].
- [35] S. Pina-Otey, V. Gaitan, F. S  nchez and T. Lux, “*Exhaustive neural importance sampling applied to Monte Carlo event generation*”, *Phys. Rev. D* **102** (2020) 013003, [arXiv:2005.12719](#) [SEMANTIC SCHOLAR].
- [36] C. Gao, S. H  che, J. Isaacson, C. Krause and H. Schulz, “*Event Generation with Normalizing Flows*”, *Phys. Rev. D* **101** (2020) 076002, [arXiv:2001.10028](#) [SEMANTIC SCHOLAR].
- [37] T. A. Le, A. G. Baydin and F. Wood, “*Inference Compilation and Universal Probabilistic Programming*”, in *Proceedings of the 20th International Conference on Artificial Intelligence and Statistics*, A. Singh and J. Zhu, eds., vol. 54 of *Proceedings of Machine Learning Research*, pp. 1338–1348, PMLR, 20–22 apr, 2017, [arXiv:1610.09900](#) [SEMANTIC SCHOLAR].
- [38] G. Papamakarios, E. Nalisnick, D. J. Rezende, S. Mohamed and B. Lakshminarayanan, “*Normalizing Flows for Probabilistic Modeling and Inference*”, *J. Mach. Learn. Res.* **22** (2022) 1, [arXiv:1912.02762](#) [SEMANTIC SCHOLAR].
- [39] A. Butter, T. Heimel, S. Hummerich, T. Krebs, T. Plehn, A. Rousselot et al., “*Generative Networks for Precision Enthusiasts*”, [arXiv:2110.13632](#) [SEMANTIC SCHOLAR].
- [40] R. Verheyen, “*Event Generation and Density Estimation with Surjective Normalizing Flows*”, *SciPost Phys.* **13** (2022) 047, [arXiv:2205.01697](#) [SEMANTIC SCHOLAR].
- [41] C. Krause and D. Shih, “*CaloFlow: Fast and Accurate Generation of Calorimeter Showers with Normalizing Flows*”, [arXiv:2106.05285](#) [SEMANTIC SCHOLAR].
- [42] C. Krause and D. Shih, “*CaloFlow II: Even Faster and Still Accurate Generation of Calorimeter Showers with Normalizing Flows*”, [arXiv:2110.11377](#) [SEMANTIC SCHOLAR].
- [43] C. Gao, J. Isaacson and C. Krause, “*i-flow: High-dimensional Integration and Sampling with Normalizing Flows*”, *Mach. Learn. Sci. Tech.* **1** (2020) 045023, [arXiv:2001.05486](#) [SEMANTIC SCHOLAR].
- [44] B. Nachman and D. Shih, “*Anomaly Detection with Density Estimation*”, *Phys. Rev. D* **101** (2020) 075042, [arXiv:2001.04990](#) [SEMANTIC SCHOLAR].
- [45] T. Golling, S. Klein, R. Mastandrea and B. Nachman, “*FETA: Flow-Enhanced Transportation for Anomaly Detection*”, [arXiv:2212.11285](#) [SEMANTIC SCHOLAR].
- [46] S. Caron, L. Hendriks and R. Verheyen, “*Rare and Different: Anomaly Scores from a combination of likelihood and out-of-distribution models to detect new physics at the LHC*”, *SciPost Phys.* **12** (2022) 077 [SEMANTIC SCHOLAR].
- [47] M. Bellagente, A. Butter, G. Kasieczka, T. Plehn, A. Rousselot, R. Winterhalder et al., “*Invertible Networks or Partons to Detector and Back Again*”, *SciPost Phys.* **9** (2020) 074, [arXiv:2006.06685](#) [SEMANTIC SCHOLAR].
- [48] M. Backes, A. Butter, M. Dunford and B. Malaescu, “*An unfolding method based on conditional Invertible Neural Networks (cINN) using iterative training*”, [arXiv:2212.08674](#) [SEMANTIC SCHOLAR].
- [49] L. Dinh, J. Sohl-Dickstein and S. Bengio, “*Density estimation using Real NVP*”, in *International Conference on Learning Representations*, 2017, [arXiv:1605.08803](#) [SEMANTIC SCHOLAR].

- [50] G. Papamakarios, T. Pavlakou and I. Murray, “*Masked Autoregressive Flow for Density Estimation*”, in *Advances in Neural Information Processing Systems*, I. Guyon, U. V. Luxburg, S. Bengio, H. Wallach, R. Fergus, S. Vishwanathan et al., eds., vol. 30, Curran Associates, Inc., 2017, [arXiv:1705.07057](#) [SEMANTIC SCHOLAR].
- [51] C. Durkan, A. Bekasov, I. Murray and G. Papamakarios, “*Neural Spline Flows*”, in *Proceedings of the 33rd International Conference on Neural Information Processing Systems*, Curran Associates Inc., Red Hook, NY, USA, 2019, [arXiv:1906.04032](#) [SEMANTIC SCHOLAR].
- [52] I. Kobyzev, S. J. Prince and M. A. Brubaker, “*Normalizing Flows: An Introduction and Review of Current Methods*”, *IEEE Transactions on Pattern Analysis and Machine Intelligence* **43** (2021) 3964 [SEMANTIC SCHOLAR].
- [53] D. P. Kingma, T. Salimans, R. Jozefowicz, X. Chen, I. Sutskever and M. Welling, “*Improved Variational Inference with Inverse Autoregressive Flow*”, in *Proceedings of the 30th International Conference on Neural Information Processing Systems*, NIPS’16, p. 4743–4751, Curran Associates Inc., Red Hook, NY, USA, 2016, [arXiv:1606.04934](#) [SEMANTIC SCHOLAR].
- [54] M. Germain, K. Gregor, I. Murray and H. Larochelle, “*MADE: Masked Autoencoder for Distribution Estimation*”, in *Proceedings of the 32nd International Conference on Machine Learning*, arXiv, 2015, [arXiv:1502.03509](#) [SEMANTIC SCHOLAR].
- [55] J. A. Gregory and R. Delbourgo, “*Piecewise Rational Quadratic Interpolation to Monotonic Data*”, *IMA Journal of Numerical Analysis* **2** (1982) 123 [SEMANTIC SCHOLAR].
- [56] Code repository for this paper on GITHUB .
- [57] NF4HEP code repository on GITHUB .
- [58] J. H. Friedman, “*On multivariate goodness-of-fit and two-sample testing*”, *Statistical Problems in Particle Physics, Astrophysics, and Cosmology* **1** (2003) 311.
- [59] R. Kansal, A. Li, J. Duarte, N. Chernyavskaya, M. Pierini, B. Orzari et al., “*On the Evaluation of Generative Models in High Energy Physics*”, [arXiv:2211.10295](#) [SEMANTIC SCHOLAR].
- [60] R. T. D’Agnolo, G. Grosso, M. Pierini, A. Wulzer and M. Zanetti, “*Learning multivariate new physics*”, *Eur. Phys. J. C* **81** (2021) 89, [arXiv:1912.12155](#) [SEMANTIC SCHOLAR].
- [61] P. Chakravarti, M. Kuusela, J. Lei and L. Wasserman, “*Model-Independent Detection of New Physics Signals Using Interpretable Semi-Supervised Classifier Tests*”, [arXiv:2102.07679](#) [SEMANTIC SCHOLAR].
- [62] M. Letizia, G. Losapio, M. Rando, G. Grosso, A. Wulzer, M. Pierini et al., “*Learning new physics efficiently with nonparametric methods*”, *Eur. Phys. J. C* **82** (2022) 879, [arXiv:2204.02317](#) [SEMANTIC SCHOLAR].
- [63] L. Del Debbio, J. M. Rossney and M. Wilson, “*Machine Learning Trivializing Maps: A First Step Towards Understanding How Flow-Based Samplers Scale Up*”, *PoS LAT-TICE2021* (2022) 059, [arXiv:2112.15532](#) [SEMANTIC SCHOLAR].
- [64] TENSORFLOW PROBABILITY MAF documentation.